Polímeros
ISSN 1678-5169 (Online)

https://doi.org/10.1590/0104-1428.20220102

ORIGINAL ARTICLE

Synergistic electrochemical method to prepare graphene oxide/polyaniline nanocomposite

Eric Luiz Pereira[1], Anderson Gama[1], Maria Elena Leyva González[1]* and Adhimar Flávio Oliveira[1]

[1]Universidade Federal de Itajubá – UNIFEI, Itajubá, MG, Brasil
**mariae@unifei.edu.br*

Abstract

Graphene oxide (GO) was electropolymerized with polyaniline (PANI) during graphite exfoliation in 0.1 M H_2SO_4 electrolyte and 0.1 M aniline monomer solution. Characterization techniques, including Infrared Absorption Spectroscopy (FTIR), Thermogravimetric Analysis (TGA), UV-vis spectroscopy, X-ray diffraction (XRD), Scanning Electron Microscopy (SEM), and cyclic voltammetry, were utilized. XRD analysis confirmed GO multilayer exfoliation from the graphite anode, while UV-vis and FTIR techniques confirmed PANI electropolymerization. SEM images revealed PANI distributed between GO multilayers with a nanoneedle morphology. Cyclic voltammetry in 1 M H_2SO_4 demonstrated that the GO/PANI composite achieved a specific capacitance of 117.440 Fg^{-1}, in contrast to GO's 1.243 Fg^{-1}, both at a scan rate of 1 mVs^{-1}. This enhancement is attributed to the improved electrical conductivity from PANI and graphene oxide. These results highlight the potential of the GO/PANI composite for high-performance supercapacitors and energy storage systems.

Keywords: *graphene oxide, electrochemical exfoliation, polyaniline, electropolymerization, nanocomposites.*

How to cite: Pereira, E. L., Gama, A., González, M. E. L., & Oliveira, A. F. (2023). Synergistic electrochemical method to prepare graphene oxide/polyaniline nanocomposite. *Polímeros: Ciência e Tecnologia*, *33*(3), e20230036. https://doi.org/10.1590/0104-1428.20220102

1. Introduction

Supercapacitors are promising energy storage devices and have attracted considerable attention in recent years[1-3]. Due to the pursuit of reducing pollution through electric vehicles, or the explosive growth of portable electronic devices, there has been a boost in the development of high-performance supercapacitors[3-5].

In this context, there are currently two main classes of electrochemical capacitors based on their charging and storage mechanism: (a) electrical double-layer capacitors in which the capacitance arises from the separation of charges at the electrode/electrolyte interface[6] and (b) redox where the pseudocapacitance arises from faradic reactions occurring at the electrode/electrolyte interface[7,8]. Large surface area carbons, noble metal oxides, and conductive polymers are the main families of materials used as electrodes in supercapacitors[9]. Conductive polymers have been widely studied, among the main conductive polymeric materials that have been investigated for application as an electrode of a supercapacitor are polyaniline (PANI)[10], polypyrrole (PPY)[11], polythiophene (PTH) and its derivatives[12].

Among these polymers, PANI is considered the most promising material due to its high capacitance, low cost, and ease of synthesis[13]. However, it can undergo expansion and contraction in volume and have low stability and easy collapse in loading and unloading, which restricts its practical applications[14]. To overcome these disadvantages, various carbon materials such as porous carbon, mesoporous carbon, and carbon nanotubes were investigated for having good conductivity, stable physicochemical properties, low cost, and long life cycle[15,16].

Another promising candidate for the fabrication of supercapacitor electrode materials is graphene oxide (GO) [17-20]. GO can be obtained from electrochemical exfoliating graphite[21]. The surface of GO contains a large number of functional groups (carboxyl, hydroxyl, epoxy group, etc.)[22]. These unique functional groups make it disperse and hydrophilic in water. In addition, GO also has a large specific surface area, broad chemical potential, excellent chemical stability, and rich[23,24] coverage morphology. In this way, graphene oxide can improve the conductivity and chemical stability of the polymer. The combination of nanometer-sized and nanostructured GOs with PANI is a promising topic for research for application in charge storage devices. GO and PANI are compatible materials due to both having conjugated π electrons. GO/PANI nanocomposite has excellent electrical properties that are linked to the large surface area of GO will allow these materials to withstand large current densities[25].

Several articles have reported the preparation of GO/PANI nanocomposite. The one-step electrochemical polymerization of a thin film of PANI/GO was reached by anodic deposition from an electrolytic solution acid of GO and aniline[25]. Other two methods are reported such as chemical polymerization of PANI in an aqueous dispersion

of GO[26-29], and by physical mixing of the GO and PANI powders dispersed in EtOH[30,31]. The present paper shows a new synthesis route to prepare GO/PANI nanocomposite. The synergistic method consists of the electrochemical polymerization of aniline by the potentiostatic method during the exfoliation of an anode electrode constituted by a graphite bar.

Thereby, this work presents the results of research whose objective was to obtain a nanocomposite of GO and PANI by electrochemical means using a synergistic method. This simple and inexpensive technique avoids polluting reagents. The procedure allows obtaining the GO/PANI nanocomposite in just a single synthesis step, from the electrosynthesis of polyaniline during the electrochemical exfoliation of graphite. The materials obtained were analyzed by morphological, physical-chemical characterization techniques, and the electrochemical performance of the materials as an electrode for supercapacitors showed promising results for application in charge storage devices.

2. Materials and Methods

2.1 Preparation of GO and GO/PANI nanocomposites

The synergistic method consists of the potentiostatic electropolymerization of PANI at the same electrode where occurs the electrochemical exfoliation of graphite to obtain graphene oxide (GO) in an electrolytic cell. This two-electrode cell has commercially sourced 8B graphite electrodes, such as anode and cathode. The electrodes were immersed in an electrolytic solution of 0.1 M sulfuric acid containing 0.1 M of aniline monomer.

The electrochemical exfoliation of the graphite electrode (anode) was performed by applying a DC voltage of +5 V for 5 min, then increasing +2 V for 5 min until reaching +13 V, using an Instrutherm Model FA-3005 Digital power supply. Simultaneously the anode was electropolymerized the PANI by a modified potentiostatic method in the same potential window from +5 V to +13 V. It was observed the appearance of bubbles and the increase of the applied tension the formation of foam on the surface of the solution. Then the foam (GO/PANI) was extracted from the electrolysis cell filtered and washed with distilled water until neutral pH and dried in an oven at 100ºC for 24h.

Electrochemical exfoliation of graphite to obtain GO was carried out under the same conditions without adding aniline to the solution. Was also noticed the appearance of bubbles and with the increase of the applied tension the formation of foam on the surface of the solution.

The filtered GO and GO/PANI were dispersed in 0.1 M sulfuric acid its solutions were used to carry out the absorbance measurements by UV-vis. The powder obtained was used for characterizations (TGA, FTIR, SEM and XRD). The same resulting powder was dissolved in dimethylsulfoxide, the solution was poured onto ITO glass to form films characterized by cyclic voltammetry.

2.2 Samples characterization

The absorbance measurements for the solutions containing dispersions of GO and GO/PANI in 0.1 M sulfuric acid was performed between 200 nm and 800 nm, using a Varin spectrometer, model: Cary 50 Bio in a quartz cuvette with a width of 10~mm and a capacity of 3.5 mL.

Thermogravimetric analysis (TGA) was performed to verify the thermal behavior of GO and GO/PANI regarding thermal degradation temperatures and mass losses. For this, the TGA-50 Shimadzu equipment was used, with samples of mass 0.2mg, in the temperature range of 25-800ºC with a heating rate of 20ºC/min, in a nitrogen atmosphere at a flow rate of 50 mL/min.

The samples were KBr pellets and then characterized at room temperature by Fourier transform infrared spectroscopy (FTIR) using the Shimadzu spectrometer, model IR Tracer 100, in the region of 600-4000 cm^{-1} with a resolution of 4 cm^{-1}.

Scanning electron microscopy (SEM) was performed with the Superscan SSX-550 SEM-EDX equipment (Shimadzu Corporation), with an electron beam of 15 kV, and coupled to an energy dispersive spectroscopy (EDS) analyzer. In the equipment, the samples (powder form) were fixed to support by double-sided carbon tape and previously metalized with gold in an IC-50 ion coater equipment (Shimadzu).

The characterization of XRD was performed by the Panalytical X'Pert Pro equipment that uses a beam of wavelength equal to 0.154 nm, provided by an Analytical Expert Diffractometer, The analysis was performed by XRD - X'Expert PRO, using CuKαwith λ= 1.505Å, at 40 kV and with a current of 40 mA. The 2θ range used was between 10-65º, with a step size of 2º/min.

Raman spectroscopy was realized at room temperature in a spectrometer Jobin-Yvon-64000 micro-Raman system, using a green laser (λ= 532 nm) as an excitation source.

For the cyclic voltammetry (CV) analysis, the potentiostat (Metrohm Autolab) was used to control such equipment, using the NOVA 2.0 Software. Cyclic voltammetry curves were performed to verify the performance of the GO/PANI and GO films for their capacitance[32]. The electrochemical cell was assembled with a conventional three-electrode system: an ITO plate modified with the GO and GO/PANI composite as the working electrode, an Ag/AgCl electrode as the reference electrode, and a Pt wire as the auxiliary electrode. The CV measurements were recorded in 0.1 M H_2SO_4, in the potential range from -0.2 V to 1.0 V, using a different scan rate of 1, 2, 3, 4, and 5 mV/s.

3. Results and Discussions

Figure 1 illustrates the potential program used for synergistic electrochemical exfoliation of graphite and electropolymerization of PANI. The increase of voltage between the working electrode (anode) and the against electrode (cathode) over time proved to be suitable for the electrochemical polymerization of PANI[33].

During the electrochemical polymerization of aniline generally, the polymer is deposited on the working electrode. The accepted mechanism reaction consists of oxidation of the monomer at the anode leading to the formation of aniline cation radicals (rate-determining step). Followed by the formation of soluble oligomers next to the electrode. Through a nucleation process, these oligomers are deposited

on an electrode. The next stage of polymerization is the propagation chain, which allows the deposition of PANI on the electrode[33].

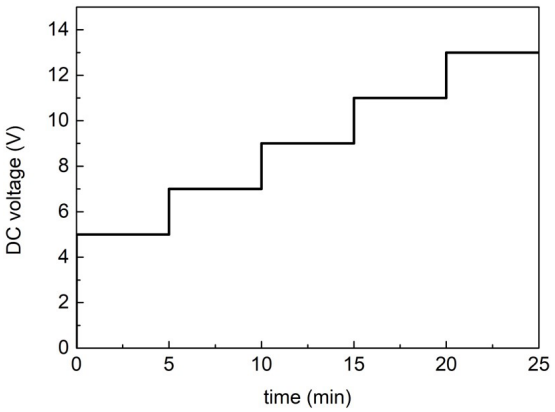

Figure 1. Schematic representation of the potential program used for the preparation of the GO/PANI nanocomposite

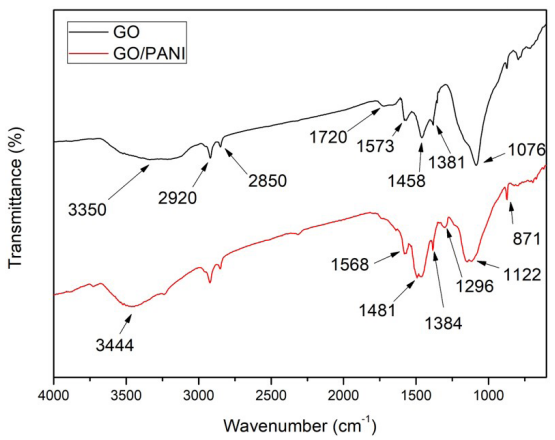

Figure 2. FTIR transmittance spectrum of GO and GO/PANI. The spectrum shows the characteristic stretching of the vibration bands at 1568 cm^{-1} (C = C, quinoid rings),1481 cm^{-1} (C = C, benzenoid rings), 1296 cm^{-1} (CN), and 1122 cm^{-1} (CH).

In our work due to higher initial potential (5V) the rate of formation of aniline cation radicals is favored and synthetized oligomers are rapidly stabilized by the nanosheets of GO. Therefore, the nucleation on the working electrode is not possible and the polymerization of PANI continues between the nanosheets of GO.

FTIR spectroscopy was used to structurally characterize the product of electrochemical exfoliation of graphite and in situ, electropolymerizations of polyaniline in GO leaves.

Figure 2 displays the spectra obtained from GO and GO/PANI. In the FTIR spectrum of the GO sheets, the presence of oxygen is observed, containing the functional groups in GO. The high-intensity band at 1076 cm^{-1} corresponds to the C-O-C stretch vibration. The band at 1381 cm^{-1} corresponds to the C-OH stretch. The peak at 1458 cm^{-1} corresponds to the splitting vibration of the O-H bond of the C-OH group. The stretching vibration of the aromatic rings (C=C) corresponds to the absorption band at 1573 cm^{-1}. The low-intensity band at 1720 cm^{-1} corresponds to the stretching vibration of the C=O bond, in the -COOH group. Note two bands 2850 cm^{-1} and 2920 cm^{-1} corresponding to the vibration of stretching C-H bonds. The widest band at 3350 cm^{-1}, corresponding to the O-H stretching vibrations, suggests that the GO sample contains a large amount of adsorbed water molecules. The FTIR spectrum of graphene oxide shows that the product, obtained by electrochemical exfoliation of graphite, is strongly oxidized and consists mainly of -OH and other oxygen-containing functional groups[34].

The FTIR spectrum of the GO/PANI product shows the characteristic vibration bands of the PANI[35] chemical structure. The broadband at 3444 cm^{-1} corresponds to the stretching vibration of the N-H bond. The spectrum shows the characteristic stretching of the vibration bands at 1568 cm^{-1} (C = C, quinoid rings), 1481 cm^{-1} (C = C, benzenoid rings), 1296 cm^{-1} (CNC), and 1122 cm^{-1} (C-NH-C). All these bands indicate the presence of PANI in the GO/PANI compound.

Figures 3a and 3b show the TGA and DTG results of the GO and GO/PANI samples degraded between 25 to 800ºC to 20ºC/min, under a nitrogen atmosphere. The TGA curves show a similar decomposition profile in both samples, in three degradation steps. The TGA and DTG curve of the GO

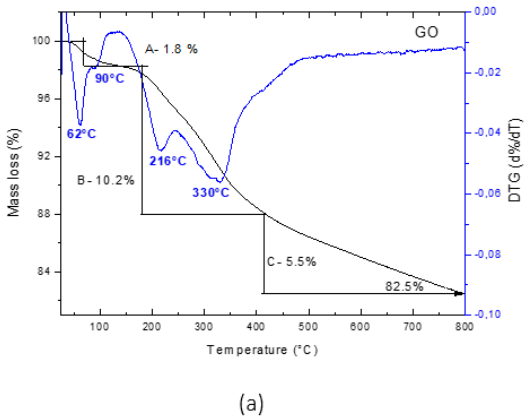

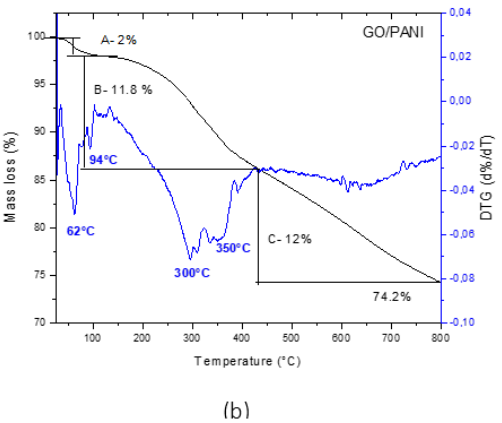

Figure 3. TGA and DTG results from (a) GO and (b) GO/PANI samples degraded between 25 to 800ºC to 20ºC/min, under a nitrogen atmosphere.

is shown in Figure 3a. It is observed that under a nitrogen atmosphere the GO degrades in three well-defined steps in the TGA curve:

- step A, temperatures ≤ 100ºC refer to water loss (1.8%);
- Step B, between 100ºC and 414ºC, refers to the loss of oxygen-containing functional groups (10.2%);
- Stage C, between 414ºC and 800ºC (slow and soft loss) attributed to the loss of oxygen functional groups with greater thermal stability (5.5%).

According to the literature, in a nitrogen atmosphere, there is no breakage of the C-C bond, related to graphene pyrolysis[36]. Finally, up to 800ºC, the TGA curve shows a residual of 82.5%.

It can be observed in Figure 3a (DTG curve) that steps A and B, described above, have the following singularities:

- Step A: two peaks of maximum degradation velocity at a temperature of 62ºC and 90ºC, We can then distinguish two types of water, one adsorbed on the surface and the other located between graphene sheets;
- Two peaks of maximum degradation velocity at temperatures of 216ºC and 330ºC, which must be related to the loss of different oxygen functional groups on the surface of graphene.

Therefore, step B which corresponds to the highest mass loss of 10.2% is due to the decomposition of oxygen-containing functional groups (such as C-OH, COC, -COOH) producing CO_2, CO, and H_2O that are removed from the GO nanosheets. These functional groups, like -COOH and -OH, on the surface of the GO not only increase dispersibility but can also anchor PANI to the surface[37].

In Figure 3b the TGA and DTG curves of GO/PANI are observed. This sample has a slightly higher moisture content (2%) and is similar to stage A of the GO. Degradation step B, between 150ºC and 430ºC, also shows a higher mass loss (11.8%). In this second step, in addition to the loss of the oxygen functional groups attached to the surface of the GO, we have the loss of mass of the PANI dopant (SO_4^{2-}). In step C, ≤ 430ºC, large mass loss occurs (12%) due to the decomposition of PANI in the GO/PANI nanocomposite. In this last step, the loss of stable oxygen functional groups linked to the GO also occurs. Finally, at 800ºC we have a residue of 74.2%, which we attribute to the GO and stable structures of the PANI, formed during the degradation.

To observe the surface of the GO/PANI nanocomposite more distinctly, SEM images were obtained for comparison. The results are shown in Figure 4.

As shown in Figure 4a, GO leaves were observed. Figure 4b shows that PANI was well distributed on the surface of GO sheets with high porosity. It is also possible to identify the PANI in nanoneedles structure in some regions of the GO surface, with an average length of approximately 0.032±0.004 μm. In agreement with some reported references[35].

When analyzing the morphology of the GO/PANI nanocomposite (Figure 4b), it is important to consider the electrical transport of the GO/PANI composite is related to the binding mechanism stated between GO and aniline monomer during electrochemical synthesis. The strong affinity between the negatively charged carboxyl group and positively charged amine nitrogen groups makes the PANI fibers bond tightly with the GO nanosheets. The aniline monomer is first adsorbed on the surface of the GO nanosheets, during the formation of PANI nanofiber under the GO nanosheets due to electrostatic attraction.

The electrochemical oxidation of aniline results in the nanostructured product shown in Figure 4b. Therefore, GO nanosheets can be considered as a support material, providing a large number of active sites for PANI growth.

The X-Ray Diffraction Spectrum for GO/PANI nanocomposite is shown in Figure 5. The first peak at $2\theta = 6.46^o$ is characteristic of Graphene Oxide and refers to the (001) plane. Compared to the literature ($2\theta = 10.2^o$ and spacing between GO sheets, d = 8.65 Å) this detachment is approximately 5.39º[38].

In the diffractogram of Figure 5, it is also possible to notice two peaks at $2\theta = 20.85^o$ and 26.515º. These peaks refer respectively to the (021) and (200) planes, which

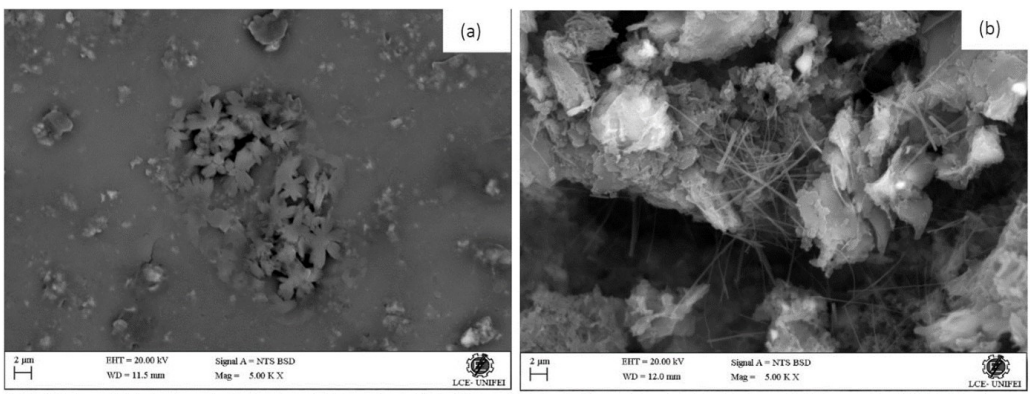

Figure 4. Comparative SEM images of (a) GO and (b) GO/PANI nanocomposite. (a) GO leaves can be observed. (b) shows that PANI was well distributed on the surface of GO sheets with high porosity. It is also possible to identify the PANI in a nanoneedles structure in some regions of the GO surface, with an average length of approximately 0.032±0.004 μm.

are characteristic of PANI and prove the polymerization of polyaniline in the material. This also suggests that the polymer on the GO surface has the same crystal structure as PANI when pure.

Figure 6 shows the UV-vis spectrum measured in 0.1 M sulfuric acid of GO/PANI and GO. An absorption peak at 314 nm is observed in the GO spectrum, which is related to the excitation n – π* transition of the carbonyl group (C=O).

In the GO/PANI spectrum, the presence of three peaks is noted. The peak at 340 nm can be linked to π - π* transitions within the benzoid ring compound. The third widest peak at 540 nm, due to PANI, originates from the cationic charged species, which are known as polarons. Furthermore, the appearance of this peak indicates that the resulting product contains polyaniline.

Through the UV-vis spectrophotometry technique, it was also possible to calculate the value of the optical

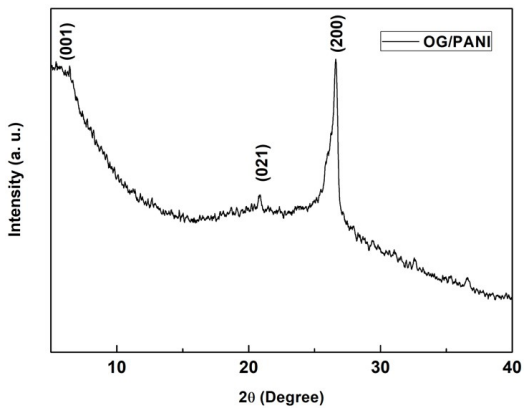

Figure 5. GO/PANI XRD spectrum. The first peak at 2 θ = 6.46º is characteristic of Graphene Oxide and refers to the (001) plane. Two peaks at 2 θ = 20.85º and 26.515º are characteristic of PANI and refer to planes (021) and (200), respectively. These peaks confirm the polymerization of polyaniline in the material.

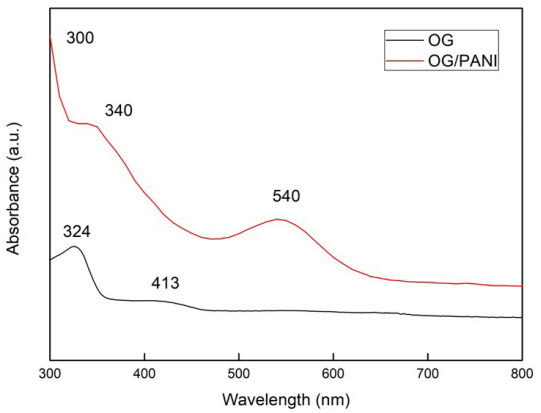

Figure 6. UV-Vis of GO/PANI and GO dispersion in 0.1 Molar sulfuric acid. In the GO/PANI spectrum, the presence of two peaks is noted. The peak is 340 nm due to a π - π* electronic transition within the benzoid ring.

bandgap (E_g). The estimate of the E_g was determined from the absorption coefficient using the Wood-Tauc equation[39]. Figure 7 shows the estimate of the indirect bandgap (n = 1/2) for the GO/PANI compound. It is observed that the G/PANI presents an indirect bandgap E_g of 2.06 eV. Figure 7 shows the estimate of the direct bandgap (n = 2) for GO/NIAP. A direct E_g of 3.01 eV can be observed for GO/PANI. It is possible to observe that GO has a direct gap E_g of 3.53 eV. The indirect gap for GO is shown in Figure 7, where an indirect gap of E_g of 3.29 eV was found.

Figure 8 shows comparatively the Raman spectra of GO and GO/PANI nanocomposite. Raman spectrum of GO displays the typical peaks at 1350 and 1600 cm^{-1}, assigned to the D band (disordered GO structure, carbon atom hybridized sp^3 due to chemical functionalization) and G band (organized hexagonal structure, carbon atom hybridized sp^2), respectively. The intensity ratio between these two bands (I_D/I_G) is a signal of the degree of disorder of the carbon structure[40]. The I_D/I_G ratio of 0.8 to GO it is agrees with the value observed in graphene oxide obtained by the electrochemical method[41].

For GO/PANI the I_D/I_G ratio shows a lower value. Like results were observed in the GO/PANI composite prepared by chemical method[42]. The interaction between GO and PANI can be by π-π stacking, electrostatic interactions, and hydrogen bonding[43]. The Raman spectrum of GO/PANI displays two new bands between D and G bands of graphene oxide, a band at 1408 cm^{-1} and a shoulder to 1533 cm^{-1}, both are assigned to the PANI backbone[44]. The performance of GO/PANI and GO Films deposited in ITO were analyzed through the cyclic voltammetry technique. These films were used as electrodes and the specific capacitance C_e in (F/g) was calculated from the results obtained using Equation 1.

$$C_e = \frac{\int_{E_1}^{E_2} i(E)\,dE}{2(E_2 - E_1)\,mv'} \quad (1)$$

where $i(E)$ is the current (A), $\int_{E_1}^{E_2} i(E)\,dE$ and the total voltammetric charge obtained by integrating positive and negative sweeps during cyclic voltammetry, $(E_2 - E_1)$ is the potential window (V), m is the average mass of the material in grams (g) and v' is the rate of sweep (V/s). The values of C_e calculated from the cyclic voltammetry curves for the GO and GO/PANI electrodes at different scan rates are shown in Table 1.

The CV curves of the GO/PANI and GO films on ITO were plotted with different scan rates of 1, 2, 3, 4, and 5 mV/s with the potential range from -0.2 to 1.0 V and are shown in Figure 9. All curves show the redox peak appearance and reflect the mixture of double layer and pseudocapacitance. The redox peaks originate from the faradaic reactions that occur between the surface of the electrodes and electrolytic ions. The cathodic peak at lower potential values (0.20V) can be linked to the transition leucoemeraldine/emeraldine. The anodic peak at higher potential values (0.6V) was associated with the transition emeraldine/pernigraniline[45].

The highest specific capacitance of GO/PANI is 117.440215 F/g at 1 mV/s. This is the highest C_e recorded

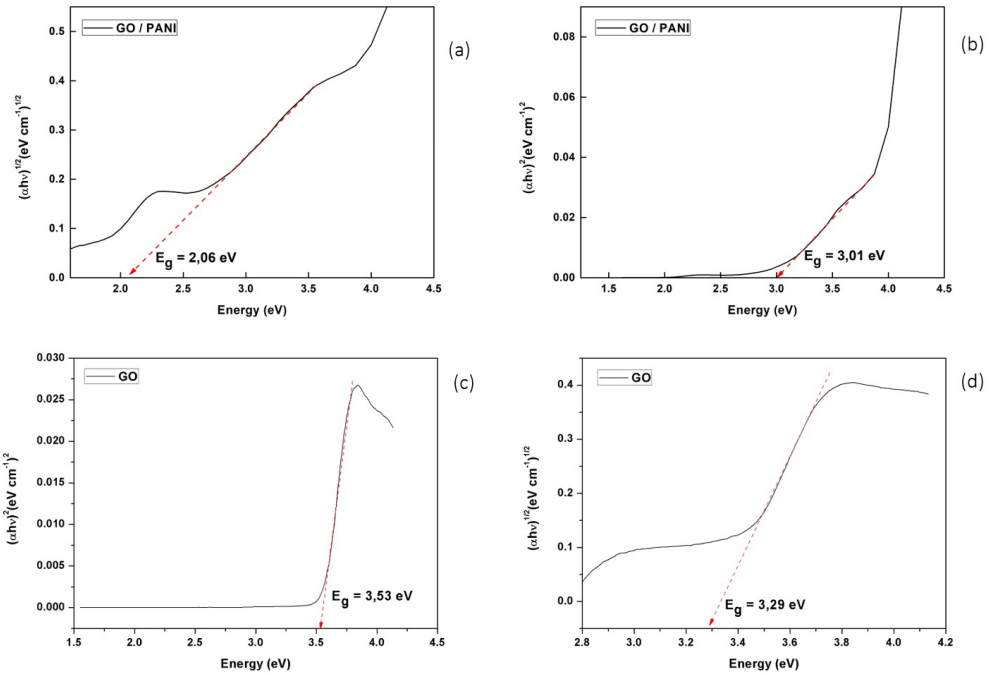

Figure 7. Tauc plot, and the respective linear extrapolation to obtain the bandwidth for the (a) indirect electronic transition of GO/PANI, (b) direct electronic transition of GO/PANI, (c) direct electronic transition of GO, and (d) indirect electronic transition of GO.

Table 1. Specific capacitance in F/g calculated from electrode cyclic voltammetry curves with GO and GO/PANI nanocomposites at different scan rates.

Scan rate (mV/s)	F/g (GO/PANI)	F/g (GO)
1	117.44	1.24
2	52.94	0.56
3	32.33	0.35
4	24.25	0.25
5	19.55	0.13

among the samples. The difference in specific capacitance is due to the highly porous nature of PANI, which provides more surface area available for redox reactions. The SEM images (Figure 4) clearly show that the GO/PANI nanocomposite film provides several microchannels for the diffusion of counter-ions during the redox reaction, which increases the accessibility in the surface area of the film. In addition, graphene oxide sheets act as Chanel in the compound and facilitate the rapid transfer of ions and electrons across the electrode surface.

Therefore, GO/PANI film shows high capacitance, even higher than some compounds. Higher values of specific capacitance of PANI were reported by some authors[46], as well as for PANI with nanoneedles morphology. The cyclic voltammetry curves of the ITO electrode deposited with GO are shown in Figure 9. The highest specific capacitance of GO is 1.24 F/g at 1 mV/s.

In both electrodes, the specific capacitance decreased with increasing scan rates. This is because the ion concentration at the electrode-electrolyte surface is increasing rapidly and

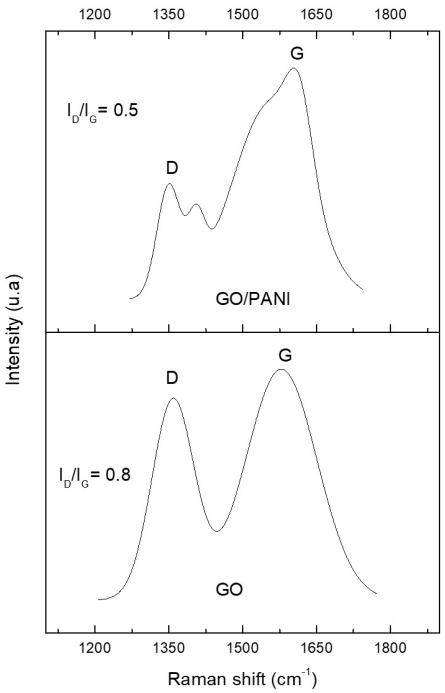

Figure 8. Raman spectra of GO and GO/PANI.

the diffusion rates of electrolyte ions at the electrode interface are still not sufficient to satisfy electrochemical reactions.

The device underwent a cyclic stability test, where it was subjected to a cyclic current of 0.3 mA for more than

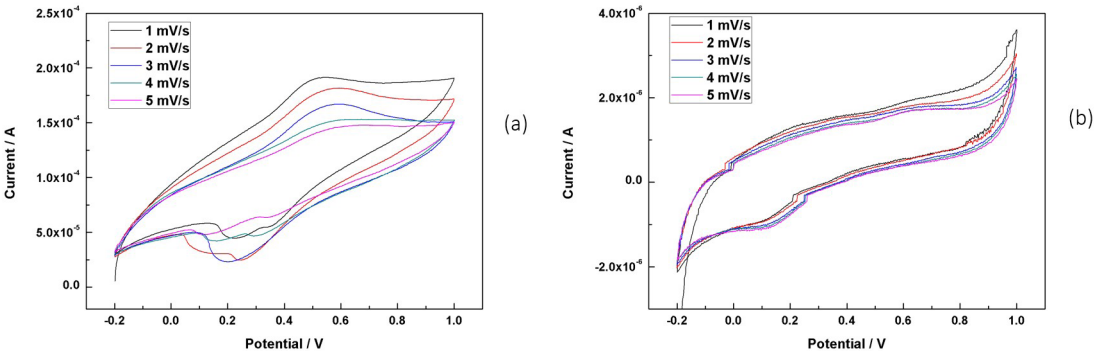

Figure 9. Cyclic voltammetry curves of the ITO electrode with (a) GO/PANI film and (b) GO film, in a solution of 1 M of H_2SO_4, with different scanning rates in the range potential from -0.2 to 1.0 V.

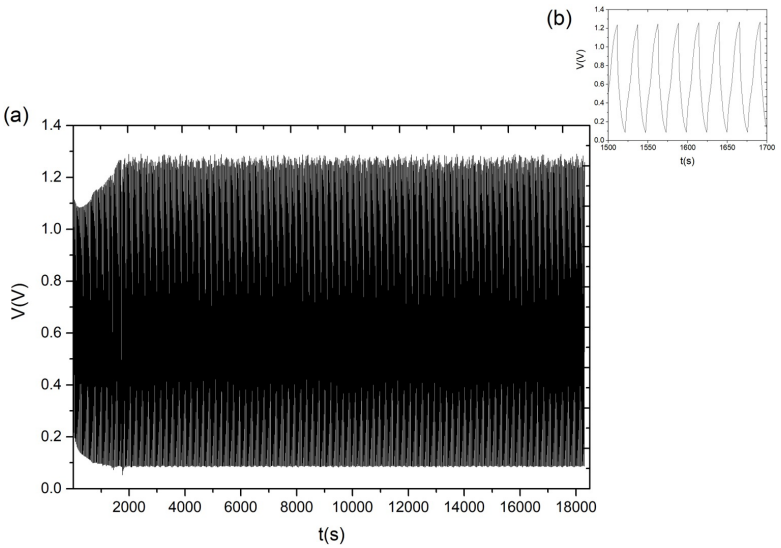

Figure 10. (a) Charging and discharging the device during an interval of more than 5h, (b) insert of Figure (a).

5 hours, with an application interval of 15 seconds followed by a discharge of 10 seconds in a load that consumed -0.3 mA (see Figure 10). To aid visualization, Figure 10b presents an excerpt from Figure 9a. Remarkably, the specific capacitance exhibited a small initial increase and subsequently maintained a constant level. This increase in specific capacitance can be attributed to insufficient contact between the composite material and the aqueous electrolyte solution during the initial stages of the electrochemical process. The initial capacitance increment is probably the result of favorable wetting of the composite materials by the electrolyte, which facilitates a reduction in the electrode's internal resistance.

In conclusion, the examined samples exhibit characteristics of graphene oxide (GO) sheets, and the GO/polyaniline (PANI) nanocomposite showcases PANI nanoneedles distributed within the GO sheets, resulting in high porosity. Despite being a cost-effective technique, it proved to be efficient, as the formation of GO was confirmed by various analyses, including TGA, FTIR, XRD, and UV-vis. Furthermore, the studied material, based on graphene oxide and polyaniline, demonstrates a high specific capacitance and excellent stability overcharge and discharge cycles. Therefore, it stands as an outstanding candidate for use in charge storage devices, such as capacitors and supercapacitors.

4. Conclusions

Composites of graphene oxide and polyaniline were successfully synthesized by a synergistic new method based on electrochemical exfoliation of graphite and potentiostatic electropolymerization of polyaniline.

The X-ray diffraction pattern confirmed the polymerization of polyaniline in the material and indicated that the introduction of the polymer in GO increased the space between the GO layers by 57%. FTIR spectroscopy provided chemical structural information on GO and GO/PANI. The FTIR spectrum of GO/PANI clearly showed the characteristic PANI bands at 1568 and 1481 cm-1. The FTIR spectrum confirmed that the surface of the GO was completely oxidized. The UV-Vis spectrum confirmed the presence of PANI through the

polaronic band. SEM image confirmed the presence of GO nanosheets and PANI nanoneedles interspersed between GO with an average length of approximately 0.032±0.004 µm distributed in the surface regions of the GO nanosheets.

Thermal characterization by thermogravimetry (TGA) showed that both the GO and the GO/PANI nanocomposite degrade in three well-defined steps. TGA showed a high content of functional groups present in the GO structure.

From the analysis of cyclic voltammetry, it is evident that the addition of PANI (GO/PANI) to GO significantly enhanced its electrochemical performance. The highest specific capacitance observed for GO/PANI was 117.44 F/g, measured at a sweep rate of 1 mV/s. Notably, this value is approximately 94.44 times greater than the specific capacitance of GO analyzed under identical conditions. Furthermore, the device demonstrated excellent performance throughout the charge and discharge tests, indicating its reliability and stability as a charge storage device. These results highlight the potential of GO/PANI as an improved material for use in energy storage applications, such as capacitors and supercapacitors. Taking into account all the characterizations performed, the material studied in this research, based on graphene oxide and polyaniline, is an excellent candidate for applications in energy storage devices, such as supercapacitors, as it has a high specific capacitance. In addition, despite being a low-cost technique, it proved to be efficient, as the formation of the GO was confirmed by both TGA and FTIR, DRX, and UV-vis. Finally, the images performed in SEM showed characteristics of GO sheets and in the GO/PANI composite, the PANI with nanoneedles morphology appears well distributed between GO sheets with high porosity.

5. Author's Contribution

• **Conceptualization –** Maria Elena Leyva González; Adhimar Flávio Oliveira.

• **Data curation –** Maria Elena Leyva González; Adhimar Flávio Oliveira.

• **Formal analysis –** Eric Luiz Pereira; Maria Elena Leyva; Anderson Gama; Adhimar Flávio Oliveira.

• **Funding acquisition –** Maria Elena Leyva González.

• **Investigation –** Eric Luiz Pereira; Maria Elena Leyva González; Anderson Gama; Adhimar Flávio Oliveira.

• **Methodology –** Eric Luiz Pereira; Maria Elena Leyva González; Anderson Gama; Adhimar Flávio Oliveira.

• **Project administration –** Maria Elena Leyva González.

• **Resources –** Maria Elena Leyva González.

• **Software –** NA.

• **Supervision –** Maria Elena Leyva González; Adhimar Flávio Oliveira.

• **Validation –** Eric Luiz Pereira; Maria Elena Leyva González; Anderson Gama; Adhimar Flávio Oliveira.

• **Visualization –** Eric Luiz Pereira; Maria Elena Leyva González; Adhimar Flávio Oliveira.

• **Writing – original draft –** Eric Luiz Pereira; Maria Elena Leyva González; Adhimar Flávio Oliveira.

• **Writing – review & editing –** Eric Luiz Pereira; Anderson Gama; Maria Elena Leyva González; Adhimar Flávio Oliveira.

6. Acknowledgements

The authors would like to thank the Brazilian agencies CAPES, CNPq, and Fapemig (Finance Code APQ-02676-16 and APQ-00010-18) for financial support.

7. References

1. Wang, H., Hao, Q., Yang, X., Lu, L., & Wang, X. (2010). Effect of graphene oxide on the properties of its composite with polyaniline. *ACS Applied Materials & Interfaces*, *2*(3), 821-828. http://dx.doi.org/10.1021/am900815k. PMid:20356287.
2. Chatterjee, D. P., & Nandi, A. K. (2021). A review on the recent advances in hybrid supercapacitors. *Journal of Materials Chemistry. A, Materials for Energy and Sustainability*, *9*(29), 15880-15918. http://dx.doi.org/10.1039/D1TA02505H.
3. Wang, Y., Zhang, L., Hou, H., Xu, W., Duan, G., He, S., Liu, K., & Jiang, S. (2020). Recent progress in carbon-based materials for supercapacitor electrodes: a review. *Journal of Materials Science*, *56*(1), 173-200. http://dx.doi.org/10.1007/s10853-020-05157-6.
4. Veerendra, A. S., Mohamed, M. R., Leung, P. K., & Shah, A. A. (2020). Hybrid power management for fuel cell/supercapacitor series hybrid electric vehicle. *International Journal of Green Energy*, *18*(2), 128-143. http://dx.doi.org/10.1080/15435075.2020.1831511.
5. Pallavolu, M. R., Nallapureddy, J., Nallapureddy, R. R., Neelima, G., Yedluri, A. K., Mandal, T. K., Pejjai, B., & Joo, S. W. (2021). Self-assembled and highly faceted growth of Mo and V doped ZnO nanoflowers for high-performance supercapacitors. *Journal of Alloys and Compounds*, *886*, 161234. http://dx.doi.org/10.1016/j.jallcom.2021.161234.
6. Yin, X., Zhang, J., Yang, L., Xiao, W., Zhou, L., Tang, Y., & Yang, W. (2022). Carbon electrodes with ionophobic characteristics in organic electrolyte for high-performance electric double-layer capacitors. *Science China Materials*, *65*(2), 383-390. http://dx.doi.org/10.1007/s40843-021-1751-x.
7. Gupta, V., & Miura, N. (2006). Polyaniline/single-wall carbon nanotube (PANI/SWCNT) composites for high performance supercapacitors. *Electrochimica Acta*, *52*(4), 1721-1726. http://dx.doi.org/10.1016/j.electacta.2006.01.074.
8. Kang, M., Jo, Y., Mun, C., Yeom, J., Park, J. S., Jung, H. S., Kim, D.-H., Park, S.-G., & Yoo, S. M. (2021). Nanoconfined 3D redox capacitor-based electrochemical sensor for ultrasensitive monitoring of metabolites in bacterial communication. *Sensors and Actuators. B, Chemical*, *345*, 130427. http://dx.doi.org/10.1016/j.snb.2021.130427.
9. Hussain, I., Lamiel, C., Ahmad, M., Chen, Y., Shuang, S., Javed, M. S., Yang, Y., & Zhang, K. (2021). High entropy alloys as electrode material for supercapacitors: a review. *Journal of Energy Storage*, *44*, 103405. http://dx.doi.org/10.1016/j.est.2021.103405.
10. Bao, L. Q., Nguyen, T.-H., Fei, H., Sapurina, I., Ngwabebhoh, F. A., Bubulinca, C., Munster, L., Bergerová, E. D., Lengalova, A., Jiang, H., Dao, T. T., Bugarova, N., Omastova, M., Kazantseva, N. E., & Saha, P. (2021). Electrochemical performance of composites made of rGO with Zn-MOF and PANI as electrodes for supercapacitors. *Electrochimica Acta*, *367*, 137563. http://dx.doi.org/10.1016/j.electacta.2020.137563.
11. Snook, G. A., & Chen, G. Z. (2008). The measurement of specific capacitances of conducting polymers using the quartz crystal microbalance. *Journal of Electroanalytical Chemistry*

(Lausanne, Switzerland), *612*(1), 140-146. http://dx.doi.org/10.1016/j.jelechem.2007.08.024.

12. Ferraris, J. P., Eissa, M. M., Brotherston, I. D., & Loveday, D. C. (1998). Performance evaluation of poly 3-(phenylthiophene) derivatives as active materials for electrochemical capacitor applications. *Chemistry of Materials*, *10*(11), 3528-3535. http://dx.doi.org/10.1021/cm9803105.
13. Heme, H. N., Alif, M. S. N., Rahat, S. S. M., & Shuchi, S. B. (2021). Recent progress in polyaniline composites for high capacity energy storage: A review. *Journal of Energy Storage*, *42*, 103018. http://dx.doi.org/10.1016/j.est.2021.103018.
14. Xu, J., Wang, K., Zu, S.-Z., Han, B.-H., & Wei, Z. (2010). Hierarchical nanocomposites of polyaniline nanowire arrays on graphene oxide sheets with synergistic effect for energy storage. *ACS Nano*, *4*(9), 5019-5026. http://dx.doi.org/10.1021/nn1006539. PMid:20795728.
15. Simon, P., & Gogotsi, Y. (2008). Materials for electrochemical capacitors. *Nature Materials*, *7*(11), 845-854. http://dx.doi.org/10.1038/nmat2297. PMid:18956000.
16. Chen, H., Li, W., He, M., Chang, X., Zheng, X., & Ren, Z. (2021). Vertically oriented carbon nanotube as a stable frame to support the Co0. 85Se nanoparticles for high performance supercapacitor electrode. *Journal of Alloys and Compounds*, *855*(Pt 2), 157506. http://dx.doi.org/10.1016/j.jallcom.2020.157506.
17. Szabó, T., Tombácz, E., Illés, E., & Dékány, I. (2006). Enhanced acidity and pH-dependent surface charge characterization of successively oxidized graphite oxides. *Carbon*, *44*(3), 537-545. http://dx.doi.org/10.1016/j.carbon.2005.08.005.
18. Li, Z. J., Yang, B. C., Zhang, S. R., & Zhao, C. M. (2012). Graphene oxide with improved electrical conductivity for supercapacitor electrodes. *Applied Surface Science*, *258*(8), 3726-3731. http://dx.doi.org/10.1016/j.apsusc.2011.12.015.
19. Yusuf, B., Hashim, M. R., & Halim, M. M. (2022). Efficiency improvement of molybdenum oxide doped with graphene oxide thin films solar cells processed by spray pyrolysis technique. *Physica B, Condensed Matter*, *625*, 413532. http://dx.doi.org/10.1016/j.physb.2021.413532.
20. Song, J., Wang, X., & Chang, C.-T. (2014). Preparation and characterization of graphene oxide. *Journal of Nanomaterials*, *276143*, 1-6. http://dx.doi.org/10.1155/2014/276143.
21. Kamata, K., Yonehara, K., Sumida, Y., Yamaguchi, K., Hikichi, S., & Mizuno, N. (2003). Efficient epoxidation of olefins with≥ 99% selectivity and use of hydrogen peroxide. *Science*, *300*(5621), 964-966. http://dx.doi.org/10.1126/science.1083176. PMid:12738860.
22. Sarangapani, S., Tilak, B. V., & Chen, C.-P. (1996). Materials for electrochemical capacitors: theoretical and experimental constraints. *Journal of the Electrochemical Society*, *143*(11), 3791-3799. http://dx.doi.org/10.1149/1.1837291.
23. Kim, J., Cote, L. J., Kim, F., Yuan, W., Shull, K. R., & Huang, J. (2010). Graphene oxide sheets at interfaces. *Journal of the American Chemical Society*, *132*(23), 8180-8186. http://dx.doi.org/10.1021/ja102777p. PMid:20527938.
24. Agarwal, V., & Zetterlund, P. B. (2021). Strategies for reduction of graphene oxide–A comprehensive review. *Chemical Engineering Journal*, *405*, 127018. http://dx.doi.org/10.1016/j.cej.2020.127018.
25. Qin, Q., He, F., & Zhang, W. (2016). One-step electrochemical polymerization of polyaniline flexible counter electrode doped by graphene. *Journal of Nanomaterials*, *2016*, 1076158. http://dx.doi.org/10.1155/2016/1076158.
26. Yan, X., Chen, J., Yang, J., Xue, Q., & Miele, P. (2010). Fabrication of free-standing, electrochemically active, and biocompatible graphene oxide− polyaniline and graphene− polyaniline hybrid papers. *ACS Applied Materials & Interfaces*, *2*(9), 2521-2529. http://dx.doi.org/10.1021/am100293r. PMid:20735069.
27. Liu, Y., Ma, Y., Guang, S., Ke, F., & Xu, H. (2015). Polyaniline-graphene composites with a three-dimensional array-based nanostructure for high-performance supercapacitors. *Carbon*, *83*, 79-89. http://dx.doi.org/10.1016/j.carbon.2014.11.026.
28. Mooss, V. A., & Athawale, A. A. (2016). Polyaniline–graphene oxide nanocomposites: influence of nonconducting graphene oxide on the conductivity and oxidation-reduction mechanism of polyaniline. *Journal of Polymer Science. Part A, Polymer Chemistry*, *54*(23), 3778-3786. http://dx.doi.org/10.1002/pola.28277.
29. Katore, M. S., Nemade, K. R., Yawale, S. S., & Yawale, S. P. (2016). Photovoltaic application of architecture ITO/graphene oxide–polyaniline/aluminum. *Journal of Materials Science Materials in Electronics*, *27*(9), 9828-9835. http://dx.doi.org/10.1007/s10854-016-5049-5.
30. Chang, T.-W., Lin, L.-Y., Peng, P.-W., Zhang, Y. X., & Huang, Y.-Y. (2018). Enhanced electrocapacitive performance for the supercapacitor with tube-like polyaniline and graphene oxide composites. *Electrochimica Acta*, *259*, 348-354. http://dx.doi.org/10.1016/j.electacta.2017.10.195.
31. Liao, C.-Y., Chien, H.-H., Hao, Y.-C., Chen, C.-W., Yu, I.-S., & Chen, J.-Z. (2018). Low-temperature-annealed reduced graphene oxide–polyaniline nanocomposites for supercapacitor applications. *Journal of Electronic Materials*, *47*(7), 3861-3868. http://dx.doi.org/10.1007/s11664-018-6260-3.
32. Beyazay, T., Oztuna, F. E. S., & Unal, U. (2019). Self-standing reduced graphene oxide papers electrodeposited with manganese oxide nanostructures as electrodes for electrochemical capacitors. *Electrochimica Acta*, *296*, 916-924. http://dx.doi.org/10.1016/j.electacta.2018.11.033.
33. Shab-Balcerzak, E. (Ed.) (2011). *Electropolymerization*. Slovakia: Intechopen. http://dx.doi.org/10.5772/1119.
34. Perumal, S., Atchudan, R., Edison, T. N. J. I., Shim, J.-J., & Lee, Y. R. (2021). Exfoliation and noncovalent functionalization of graphene surface with poly-N-vinyl-2-pyrrolidone by in situ polymerization. *Molecules (Basel, Switzerland)*, *26*(6), 1534. http://dx.doi.org/10.3390/molecules26061534. PMid:33799693.
35. Makuła, P., Pacia, M., & Macyk, W. (2018). How to correctly determine the band gap energy of modified semiconductor photocatalysts based on UV–Vis spectra. *The Journal of Physical Chemistry Letters*, *9*(23), 6814-6817. http://dx.doi.org/10.1021/acs.jpclett.8b02892. PMid:30990726.
36. Manivel, P., Dhakshnamoorthy, M., Balamurugan, A., Ponpandian, N., Mangalaraj, D., & Viswanathan, C. (2013). Conducting polyaniline-graphene oxide fibrous nanocomposites: preparation, characterization and simultaneous electrochemical detection of ascorbic acid, dopamine and uric acid. *RSC Advances*, *3*(34), 14428-14437. http://dx.doi.org/10.1039/c3ra42322k.
37. Nguyen, V. H., Tang, L., & Shim, J.-J. (2013). Electrochemical property of graphene oxide/polyaniline composite prepared by in situ interfacial polymerization. *Colloid & Polymer Science*, *291*(9), 2237-2243. http://dx.doi.org/10.1007/s00396-013-2940-y.
38. Hu, H., Wang, X., Wang, J., Wan, L., Liu, F., Zheng, H., Chen, R., & Xu, C. (2010). Preparation and properties of graphene nanosheets–polystyrene nanocomposites via in situ emulsion polymerization. *Chemical Physics Letters*, *484*(4-6), 247-253. http://dx.doi.org/10.1016/j.cplett.2009.11.024.
39. Toledo, R. P., Huanca, D. R., Oliveira, A. F., Santos Filho, S. G., & Salcedo, W. J. (2020). Electrical and optical characterizations of erbium doped MPS/PANI heterojunctions. *Applied Surface Science*, *529*, 146994. http://dx.doi.org/10.1016/j.apsusc.2020.146994.
40. Zhou, Y., Yen, C. H., Fu, S., Yang, G., Zhu, C., Du, D., Wo, P. C., Cheng, X., Yang, J., Waic, C. M., & Lin, Y. (2015).

One-pot synthesis of B-doped three-dimensional reduced graphene oxide via supercritical fluid for oxygen reduction reaction. *Green Chemistry*, *17*(6), 3552-3560. http://dx.doi.org/10.1039/C5GC00617A.

41. Jibrael, R. I., & Mohammed, M. F. A. (2016). Production of graphene powder by electrochemical exfoliation of graphite electrodes immersed in aqueous solution. *Optik (Stuttgart)*, *127*(16), 6384-6389. http://dx.doi.org/10.1016/j.ijleo.2016.04.101.
42. Wu, J., Zhang, Q., Wang, J., Huang, X., & Bai, H. (2018). A self-assembly route to porous polyaniline/reduced graphene oxide composite materials with molecular-level uniformity for high-performance supercapacitors. *Energy & Environmental Science*, *11*(5), 1280-1286. http://dx.doi.org/10.1039/C8EE00078F.
43. Vargas, L. R., Poli, A. K. S., Dutra, R. C. L., Souza, C. B., Baldan, M. R., & Gonçalves, E. S. (2017). Formation of composite polyaniline and graphene oxide by physical mixture method. *Journal of Aerospace Technology and Management*, *9*(1), 29-38. http://dx.doi.org/10.5028/jatm.v9i1.697.
44. Zhang, Y., Liu, J., Zhang, Y., Liu, J., & Duan, J. (2017). Facile synthesis of hierarchical nanocomposites of aligned polyaniline nanorods on reduced graphene oxide nanosheets for microwave absorbing materials. *RSC Advances*, *7*(85), 54031-54038. http://dx.doi.org/10.1039/C7RA08794B.
45. Medeiros, M. F. X. P., Leyva, M. E., Queiroz, A. A. A., & Maron, L. B. (2020). Electropolymerization of polyaniline nanowires on poly(2-hydroxyethyl methacrylate) coated Platinum electrode. *Polímeros: Ciência e Tecnologia*, *30*(1), e2020008. http://dx.doi.org/10.1590/0104-1428.02020.
46. Li, H., Wang, J., Chu, Q., Wang, Z., Zhang, F., & Wang, S. (2009). Theoretical and experimental specific capacitance of polyaniline in sulfuric acid. *Journal of Power Sources*, *190*(2), 578-586. http://dx.doi.org/10.1016/j.jpowsour.2009.01.052.

Received: Dec. 01, 2022
Revised: Sep. 10, 2023
Accepted: Oct. 05, 2023